Seed Robustness of Oriented Image Foresting Transform: Core Computation and the Robustness Coefficient

Anderson Carlos Moreira Tavares[✉], Hans Harley Ccacyahuillca Bejar, and Paulo André Vechiatto Miranda

Institute of Mathematics and Statistics, University of São Paulo (USP), São Paulo, SP 05508-090, Brazil
{acmt,hans,pmiranda}@ime.usp.br

Abstract. In graph-based methods, image segmentation can be seen as a graph partition problem between sets of seed pixels. The core of a seed is the region where it can be moved without altering its segmentation. The larger the core, the greater the robustness of the method in relation to its seed positioning. In this work, we present an algorithm to compute the cores of Oriented Image Foresting Transform (OIFT), an extension of Fuzzy Connectedness and Watersheds to directed weighted graphs, and compare its performance to other methods according to a proposed evaluation measure, the Robustness Coefficient. Our analysis indicates that OIFT has a good balance between accuracy and robustness, being able to overcome several methods in some datasets.

Keywords: Oriented Image Foresting Transform · Fuzzy Connectedness · Graph segmentation

1 Introduction

Image segmentation can be interpreted as a graph partition problem subject to hard constraints, given by seed pixels selected in the image domain [2,4,10,12,14]. A common framework, sometimes referred to as Generalized Graph Cut (GGC) [6,9], can roughly describe, in a unified manner, several seed-based methods, including Random Walker (RW) [14], shortest path/geodesic [13], voronoi diagram and Power Watershed (PW) [6]. In particular, the *min-cut/max-flow* algorithm, also known simply as *Graph Cut* (GC) [4,5], and some methods by the *Image Foresting Transform* (IFT) framework [13], such as *Watersheds* [12] and *Fuzzy Connectedness* [10], correspond to the ε_1- and ε_∞-minimization problems, respectively, within this framework [9]. The ε_∞-minimization methods have linear-time implementations $O(N)$ with respect to the image size N [8], or $O(N \cdot logN)$ depending on the data structure of the priority queue, while the run time for the ε_1-minimization problem is $O(N^{2.5})$ for sparse graphs [5].

Oriented Image Foresting Transform (OIFT) [17,24] and Oriented Relative Fuzzy Connectedness (ORFC) [3] extend the ε_∞-minimization problem to

directed weighted graphs. OIFT's energy formulation on digraphs makes it a
very versatile method, supporting several high-level priors for object segmen-
tation, including global properties such as connectedness [16,19], shape con-
straints [18,25] and boundary polarity [17,24], which allow the customization of
the segmentation to a given target object [15]. While the introduction of combi-
natorial graphs with directed edges on other frameworks increases considerably
the complexity of the problem [27], OIFT and ORFC still run in linear time.

   In this work, we present a formal definition and an algorithm to compute the
cores of OIFT seeds, adding another unique feature to this method, since for
most segmentation algorithms there are no known efficient ways for computing
their cores. The *cores* [1] are the regions where seeds can be moved without alter-
ing the segmentation. The cores have several practical applications. In medical
research, it is usually desirable to reduce inter- and intra-user variability in image
segmentation. In this sense, the cores provide an analytic solution to measure the
reproducibility of experiments. In this work, we propose the *Robustness Coef-
ficient* to measure the seed robustness of the methods, allowing a quantitative
analysis of this aspect.

   The cores can also be used to solve an image segmentation inverse problem,
that is, for a given segmented object how to find a set with minimum number
of seeds that produces it [1]. This can be used to find a suitable set of seeds
that assembles a given automatic segmentation result, in order to allow further
changes in the seed set to repair the segmentation interactively [21,22].

   The cores can also be employed to build powerful hybrid image segmenta-
tion approaches [3,11,28]. For instance, Tavares et al. [28] proposed a hybrid
method, denoted as $ORFC_{Core} + GC$, which combines, the strengths of ORFC
cores (robustness to the seed choice and low false-positive rate) and Graph Cut
(smoother and more regular contours, thus, avoiding "leaking though poorly
defined boundary segments").

   For the sake of completeness in presentation, Sect. 2 includes an overview
of concepts on image graph and a revision of the methods ORFC and OIFT.
Section 3 shows the proposed algorithm to compute the cores of OIFT seeds,
In Sect. 4, we evaluate OIFT and other methods according to their Robustness
Coefficient and state our conclusions.

2   Background

A digital *image* is a mapping $I : \mathcal{I} \to \mathbb{Z}$, assigning an intensity $I(s)$ to a pixel s,
where $\mathcal{I} \subset \mathbb{Z}^n$ is the image domain. An image can be interpreted as a weighted
digraph $G = \langle V, E, \omega \rangle$, whose nodes V are the image pixels ($V = \mathcal{I}$), the arcs
are the ordered pixel pairs $\langle s, t \rangle \in E$, and $\omega : E \to \mathbb{Z}$ assigns a weight to each
arc. For example, one can take E to consist of all pairs of ordered pixels $\langle s, t \rangle$
in the Cartesian product $\mathcal{I} \times \mathcal{I}$ such that the Euclidean distance $d_{\text{euc}}(s, t) \leq \rho$
and $s \neq t$, where ρ is a specified constant (e.g., 4-neighborhood, when $\rho = 1$,
and 8-neighborhood, when $\rho = \sqrt{2}$, in case of 2D images). The transpose $G^T = \langle V, E^T, \omega^T \rangle$ of G is the unique digraph where $E^T = \{\langle t, s \rangle : \langle s, t \rangle \in E\}$ and

$\omega^T(\langle s,t\rangle) = \omega(\langle t,s\rangle)$. In this work, we consider G as a *symmetric* digraph, where $\langle s,t\rangle \in E \Rightarrow \langle t,s\rangle \in E$.

A *path* $\pi_{s\rightsquigarrow t} = \langle s = t_1, t_2, \ldots, t_n = t\rangle$ is a sequence of adjacent and distinct nodes, where s stands for the *origin* and t for the *terminus*. $\Pi_{s\rightsquigarrow t}$ is the set of all paths in G from s to t, $\Pi_t = \bigcup_{s\in V} \Pi_{s\rightsquigarrow t}$ and $\Pi = \bigcup_{t\in V} \Pi_t$. We use $\Pi(G)$ to explicitly indicate all possible paths in a particular graph G. Let also $\pi_{\mathcal{S}\rightsquigarrow t} \in \Pi_{\mathcal{S}\rightsquigarrow t} = \{\pi_{s\rightsquigarrow t} : s \in \mathcal{S}\}$, for any $\mathcal{S} \subset V$. A path is *trivial* when $\pi_t = \langle t\rangle$. A path $\pi_t = \pi_s \cdot \langle s,t\rangle$ indicates the extension of a path π_s by an arc $\langle s,t\rangle$. A *predecessors map* is a function $P : V \to V \cup \{nil\}$ where $\forall t \in V, P(t) = s$ where $\langle s,t\rangle \in E$ or $s = nil$. A *spanning forest* is a predecessors map without cycles. The roots of the forest are the nodes $R^P = \{r \in V : P(r) = nil\}$. Let π_t^P be defined recursively as $\langle t\rangle$ if $t \in R^P$, and $\pi_s^P \cdot \langle s,t\rangle$ if $P(t) = s$. Let $DCC_G(s) = \{t \in V : \exists \pi_{s\rightsquigarrow t} \in \Pi(G)\}$ be the *Directed Connected Component* of basepoint $s \in V$, the set of all successors of s, and $SCC_G(s) = \{t \in V : \exists \{\pi_{s\rightsquigarrow t}, \pi_{t\rightsquigarrow s}\} \subseteq \Pi(G)\}$ the *Strongly Connected Component* of s, the set of nodes containing s where any two are connected by paths. We can relate DCC and SCC as: $SCC_G(s) = \{t \in V : s \in DCC_G(t) \text{ and } t \in DCC_G(s)\}$. A *connectivity function* $f : \Pi \to \mathbb{Z}$ assigns a value to any path $\pi \in \Pi$. A path π_t is *optimum* if $f(\pi_t) \geq f(\pi_t')$ for any other path $\pi_t' \in \Pi_t$. We denote an optimum path for t as π_t^*. This generates the *connectivity map* $C_{opt} : V \to \mathbb{Z}$ as $C_{opt}(t) = f(\pi_t^*)$.

Let $\mathcal{X} = \{\mathcal{O} : \mathcal{O} \subseteq V\}$ be the space of all possible binary segmented objects $\mathcal{O}$. A seed-based segmentation uses *seeds* $\mathcal{S} = \mathcal{S}_o \cup \mathcal{S}_b \subseteq V$, where $\mathcal{S}_o$ and $\mathcal{S}_b$ are *object* ($\mathcal{S}_o \subseteq \mathcal{O}$) and *background* ($\mathcal{S}_b \subseteq V \setminus \mathcal{O}$) seed sets, respectively. They restrict $\mathcal{X}$ to $\mathcal{X}(\mathcal{S}_o, \mathcal{S}_b) = \{\mathcal{O} \in \mathcal{X} : \mathcal{S}_o \subseteq \mathcal{O} \subseteq V \setminus \mathcal{S}_b\}$. A *cut* is defined as $\mathcal{C}(\mathcal{O}) = \{\langle s,t\rangle \in E : s \in \mathcal{O} \text{ and } t \notin \mathcal{O}\}$. We can associate an energy value $\varepsilon(\mathcal{O})$ to an object (and its cut), and restrict the set of solutions to those which minimizes it. Let energy $\varepsilon_q(\mathcal{O}) = (\sum_{\langle s,t\rangle \in \mathcal{C}(\mathcal{O})} \omega(\langle s,t\rangle)^q)^{\frac{1}{q}}$. The original Graph Cut algorithm minimizes $\varepsilon_1(\mathcal{O})$, while ORFC and OIFT minimize $\varepsilon_\infty(\mathcal{O}) = \max_{\langle s,t\rangle \in \mathcal{C}(\mathcal{O})} \omega(\langle s,t\rangle)$ [9], as presented next.

2.1   Oriented Image Foresting Transform (OIFT)

The *Image Foresting Transform* (IFT) [13] is an algorithm which takes a graph G, a connectivity function f and computes a connectivity map $C : V \to \mathbb{Z}$ defined by a spanning forest P, as $C(t) = f(\pi_t^P)$, which converges to $C_{opt}(t) = f(\pi_t^*), \forall t \in V$, when f is a *smooth* connectivity function [13].

OIFT is a ε_∞-minimization method [17,24] build upon the IFT framework. It uses the connectivity function $f^{\circlearrowright}$ (Eq. 1) in a symmetric digraph.

$$f^{\circlearrowright}(\langle t\rangle) = \begin{cases} \infty & \text{if } t \in \mathcal{S}_o \cup \mathcal{S}_b \\ -\infty & \text{otherwise} \end{cases}$$

$$f^{\circlearrowright}(\pi_{r\rightsquigarrow s} \cdot \langle s,t\rangle) = \begin{cases} \min\{f^{\circlearrowright}(\pi_{r\rightsquigarrow s}), \omega(\langle s,t\rangle) \cdot 2\} & \text{if } r \in \mathcal{S}_o \\ \min\{f^{\circlearrowright}(\pi_{r\rightsquigarrow s}), \omega(\langle t,s\rangle) \cdot 2 + 1\} & \text{otherwise} \end{cases}$$

$$(1)$$

The segmented object $A_{OIFT}(\mathcal{S}_o, \mathcal{S}_b)$ by OIFT is defined from the forest P computed by IFT with $f^{\vec{\sigma}}$, by taking as object all nodes conquered by paths rooted in $\mathcal{S}_o$, that is, $A_{OIFT}(\mathcal{S}_o, \mathcal{S}_b) = \{t \in V : \pi_t^P \in \Pi_{\mathcal{S}_o \leadsto t}\}$. The optimality of $A_{OIFT}(\mathcal{S}_o, \mathcal{S}_b)$ is given by the ε_∞-minimization problem. Although ORFC (which is described in next section) and OIFT are methods from the same energy class, their outputs are usually different with distinct characteristics (Fig. 1).
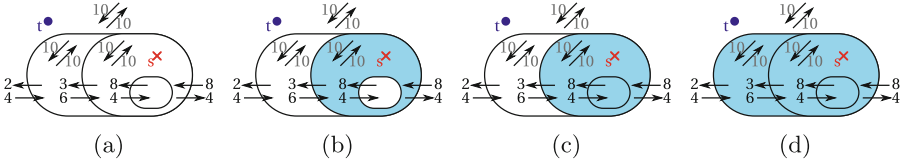

Fig. 1. (a) Input image graph with $\mathcal{S}_o = \{s\}$ and $\mathcal{S}_b = \{t\}$. (b) ORFC result. (c) A candidate solution. (d) OIFT result. Note that all the three solutions have the same energy $\varepsilon_\infty(\mathcal{O}) = 4$.

In order to explore the boundary orientation/polarity to resolve between very similar nearby boundary segments with opposite transitions (dark to bright/bright to dark), the weight $\omega(\langle s, t \rangle)$ can be defined as:

$$\omega(\langle s,t \rangle) = \begin{cases} \delta(s,t) \times (1-\alpha) & \text{if } I(s) > I(t) \\ \delta(s,t) \times (1+\alpha) & \text{if } I(s) < I(t) \\ \delta(s,t) & \text{otherwise} \end{cases} \tag{2}$$

where $\alpha \in [-1, 1]$ is an orientation factor and $\delta(s,t) = \delta(t,s)$ is an undirected similarity measure (e.g., $\delta(s,t) = K - |I(s) - I(t)|$, where K is a maximum intensity variation) [7,23]. Note that we usually have $\omega(\langle s,t \rangle) \neq \omega(\langle t,s \rangle)$ when $\alpha \neq 0$. For $\alpha > 0$, the segmentation by OIFT favors transitions from bright to dark pixels, and $\alpha < 0$ favors the opposite orientation.

2.2 Oriented Relative Fuzzy Connectedness (ORFC)

ORFC [3] is also a ε_∞-minimizer, for arcs from object to background nodes. Let $\varepsilon_\infty^\downarrow(\mathcal{S}_o, \mathcal{S}_b) = \min_{\mathcal{O} \in \mathcal{X}(\mathcal{S}_o, \mathcal{S}_b)} \{\varepsilon_\infty(\mathcal{O})\}$ and $\mathcal{X}_\infty^\downarrow(\mathcal{S}_o, \mathcal{S}_b) = \{\mathcal{O} \in \mathcal{X}(\mathcal{S}_o, \mathcal{S}_b) : \varepsilon_\infty(\mathcal{O}) = \varepsilon_\infty^\downarrow(\mathcal{S}_o, \mathcal{S}_b)\}$. For the seeds $\mathcal{S}_o$ and $\mathcal{S}_b$, A_{ORFC} is defined as follows:

$$A_{ORFC}(\mathcal{S}_o, \mathcal{S}_b) = \left[\bigcup_{s_i \in \mathcal{S}_o} A_{ORFC}(\{s_i\}, \mathcal{S}_b) \right], A_{ORFC}(\{s_i\}, \mathcal{S}_b) = \underset{\mathcal{O} \in \mathcal{X}_\infty^\downarrow(\{s_i\}, \mathcal{S}_b)}{\arg \min} |\mathcal{O}| \tag{3}$$

A_{ORFC} uses a connectivity function $f_{\min}^{\leftarrow}$ (Eq. 4), a smooth function which processes reversal (antiparallel) arcs. RFC is a particular case of ORFC when $\alpha = 0$. Algorithm 1 computes the ORFC segmentation in a symmetric digraph, where $C_{opt}(s_i) = \varepsilon_\infty^\downarrow(\{s_i\}, \mathcal{S}_b)$ (see Lemma 1 from Bejar and Miranda [3]).

$$f_{\overline{\min}}(\langle t \rangle) = \begin{cases} \infty & \text{if } t \in \mathcal{S}_b \\ -\infty & \text{otherwise} \end{cases} \quad f_{\overline{\min}}(\pi_{r \leadsto s} \cdot \langle s, t \rangle) = \min\{f_{\overline{\min}}(\pi_{r \leadsto s}), \omega(\langle t, s \rangle)\}$$

(4)

Algorithm 1. Computing $A_{ORFC}(\{s_i\}, \mathcal{S}_b)$

---

1 Get connectivity map C_{opt} with $f_{\overline{min}}$ by IFT;
2 Create $G_> = (V, E', \omega)$ from $G = (V, E, \omega)$ where
$E' = \{\langle s, t \rangle \in E : \omega(\langle s, t \rangle) > C_{opt}(s_i)\}$;
3 Return $DCC_{G_>}(s_i)$;

---

3 Seed Robustness Analysis of OIFT

Without loss of generality, we will constrain the analysis of robustness only to internal seeds, being the external seeds a completely symmetric problem. In order to define the concept of core, we must introduce the notion of seed equivalence.

Definition 1 *(Equivalent seeds). Two internal seeds s_1 and s_2 are said* equivalent *if they separately produce the same result. That is, for the given external seed set $\mathcal{S}_b$, we have that $A(\{s_1\}, \mathcal{S}_b) = A(\{s_2\}, \mathcal{S}_b)$.*

The notion of equivalent seeds introduced by Definition 1 is a binary relation $\equiv$ on the set of object nodes $A(\mathcal{S}_o, \mathcal{S}_b)$, i.e., $s_1 \equiv s_2$ if and only if s_1 and s_2 are equivalent. This relation is reflexive, symmetric and transitive, hence, it is indeed an *equivalence relation* as defined in mathematics. Therefore, the *core* of a seed s_1 is in fact the *equivalence class* of s_1 under $\equiv$, denoted $[s_1]$, which is defined as $[s_1] = \{t \in A(\{s_1\}, \mathcal{S}_b) : s_1 \equiv t\}$. We use the notation $\mathcal{N}(\{s_1\}, \mathcal{S}_b) = [s_1]$ to indicate the core of s_1 by algorithm A, and we consider $\mathcal{N}(\mathcal{S}_o, \mathcal{S}_b) = \bigcup_{s_i \in \mathcal{S}_o} \mathcal{N}(\{s_i\}, \mathcal{S}_b)$.

Algorithm 2 computes the cores $\mathcal{N}_{ORFC}(\mathcal{S}_o, \mathcal{S}_b)$ of ORFC in linear time, as proposed by Tavares et al. [28], by applying the Tarjan's algorithm in a proper subgraph derived from G, where each core $\mathcal{N}_{ORFC}(\{s_i\}, \mathcal{S}_b)$, $s_i \in \mathcal{S}_o$, corresponds to a SCC.

Algorithm 2. Computing $\mathcal{N}_{ORFC}(\mathcal{S}_o, \mathcal{S}_b)$

---

1 Get connectivity map C_{opt} with $f_{\overline{min}}$ by IFT;
2 Create $G_> = \langle V, E', \omega \rangle$ from $G = \langle V, E, \omega \rangle$ where
$E' = \{\langle s, t \rangle \in E : \omega(\langle s, t \rangle) > C_{opt}(s) \wedge C_{opt}(s) = C_{opt}(t)\}$;
3 Apply Tarjan's algorithm in $G_>$;
4 Return only SCCs which contains internal seeds;

From the theoretical relations presented in [28], we know that, for any $s_i \in \mathcal{S}_o$, $\mathcal{N}_{ORFC}(\{s_i\}, \mathcal{S}_b) \subseteq \mathcal{N}_{OIFT}(\{s_i\}, \mathcal{S}_b)$. If a pixel s_1 is equivalent to a pixel s_2 for

the OIFT algorithm (i.e., $s_1 \overset{\text{oift}}{\equiv} s_2$), and they belong to different ORFC cores (i.e., $\mathcal{N}_{ORFC}(\{s_1\}, \mathcal{S}_b) \neq \mathcal{N}_{ORFC}(\{s_2\}, \mathcal{S}_b)$), then by transitivity we have that $c \overset{\text{oift}}{\equiv} d$ for any $c \in \mathcal{N}_{ORFC}(\{s_1\}, \mathcal{S}_b)$ and $d \in \mathcal{N}_{ORFC}(\{s_2\}, \mathcal{S}_b)$. This observation allows us to drastically reduce the complexity of the OIFT core computation, allowing us to work in a Region Adjacency Graph (RAG), composed by the ORFC cores that can be fast computed, rather than working at the pixel level.

Since $\mathcal{N}_{OIFT}(\mathcal{S}_o, \mathcal{S}_b) \subseteq A_{OIFT}(\mathcal{S}_o, \mathcal{S}_b)$, we first compute $A_{OIFT}(\mathcal{S}_o, \mathcal{S}_b)$, then we compute all the ORFC cores inside the OIFT segmentation $A_{OIFT}(\mathcal{S}_o, \mathcal{S}_b)$. Figure 2 illustrates one example, showing all the ORFC cores inside the object for a given image graph (Fig. 2i). Figure 3a shows the resulting RAG, with a node for each ORFC core and one external node x for the background. The arc weights of the RAG are selected as the highest arc values interconnecting their regions.
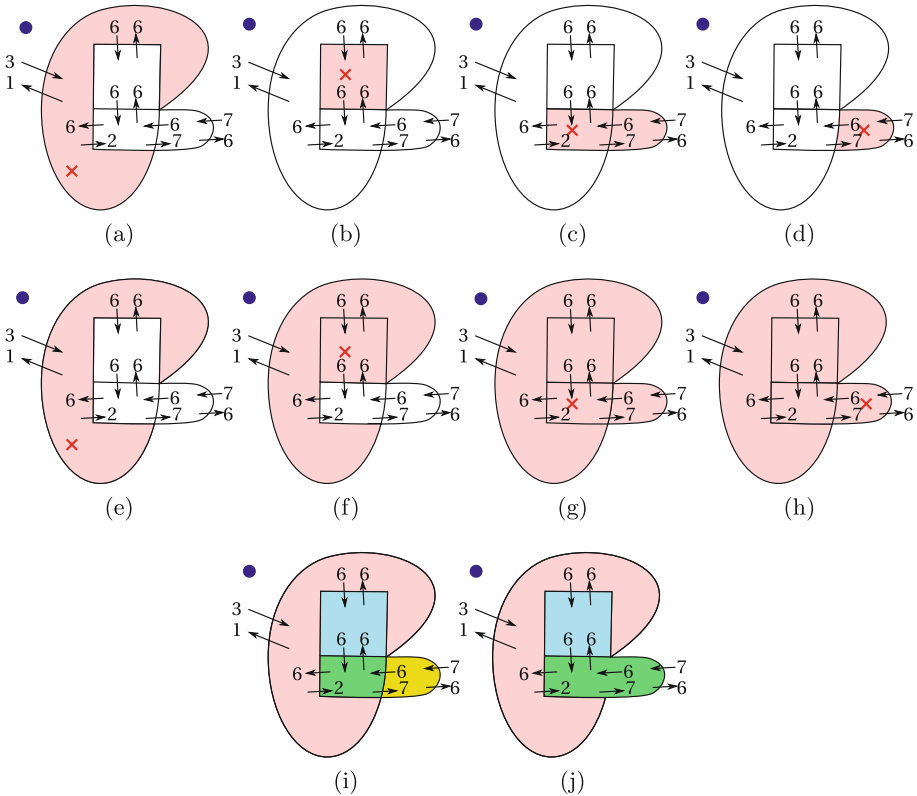

Fig. 2. (a–d) Results of ORFC, where $\omega(\langle s, t \rangle) = 10$ for non-contour edges, with a fixed external seed ● and an internal seed × in different places, (e–h) OIFT results for different internal seeds, (i) ORFC cores and (j) OIFT cores. (Color figure online)

The proposed algorithm to compute the OIFT cores uses a disjoint-set data structure. Initially, each RAG node is its own representative. For each pair $\langle c, d \rangle$, $c \neq x$ and $d \neq x$, of neighboring nodes in the RAG an equivalence test is performed and if the test is satisfied they are joined (union operation). The value $C_c(d) = f(\pi_d^*)$ of an optimum path π_d^* by the connectivity function $f_{\min}^{\longleftarrow}$ (Eq. 4) is computed in the induced subgraph $G[V \setminus \{c\}]$ from x to d (Fig. 3b). Similarly we also compute $C_d(c) = f(\pi_c^*)$ as the value of an optimum path π_c^* for $f = f_{\min}^{\longleftarrow}$ in the induced subgraph $G[V \setminus \{d\}]$ from x to c (Fig. 3c). If $\omega(\langle c, d \rangle) > C_c(d)$ and $\omega(\langle d, c \rangle) > C_d(c)$ we can conclude that $c \overset{\text{oift}}{\equiv} d$ and we perform their union operation (Fig. 3d).

In order to understand the equivalence test performed in RAG, we need to know the following property that distinguishes OIFT from ORFC. From Fig. 1, we can note that in the case of multiple solutions with the same energy, the OIFT result gives preference to boundary pieces with lower energy values. For example, between the border segments with outgoing arcs with values 3 and 2, from Fig. 1c and d, OIFT selects the one with the lowest value in Fig. 1d. This result can be verified theoretically by a proof similar to Theorem 2 (Piecewise optimum property) in [20]. In the equivalence test, $\omega(\langle c, d \rangle)$ and $C_c(d)$ essentially represent the energies of two boundary pieces. Since OIFT gives preference to lower energy values, $\omega(\langle c, d \rangle) > C_c(d)$ implies that a OIFT segmentation from a seed in c would conquer d, and $\omega(\langle d, c \rangle) > C_d(c)$ implies that d would conquer c leading to equivalent seeds. Figure 2j shows the resulting OIFT cores at the pixel level derived from the RAG in Fig. 3d.

Since we have to evaluate the equivalence test, and consequently $C_c(d)$, for all arcs $\langle c, d \rangle$ in the RAG, the final complexity of the algorithm becomes $O(|V|^2 + |E| \cdot |V|)$, where $|V|$ and $|E|$ are the number of nodes and arcs in the RAG. Note that to compute the maps C_c for all $c \in V$ requires $|V|$ IFT's executions and each IFT takes $O(|V| + |E|)$. In practice, the algorithm is fast, because the RAG has a small number of nodes compared to the image graph.
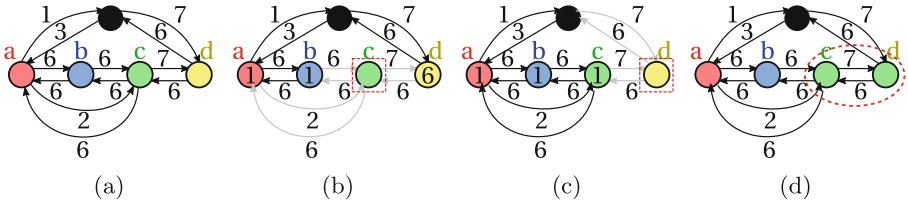

Fig. 3. (a) Region Adjacency Graph (RAG), composed by the ORFC cores from Fig. 2(b and c). The equivalence test: (b) $\omega(\langle c, d \rangle) = 7 > C_c(d) = 6$, where the values inside the nodes indicate the C_c values, and (c) $\omega(\langle d, c \rangle) = 6 > C_d(c) = 1$, where the values inside the nodes indicate C_d values. (d) The union operation.

4   Experimental Results and Conclusions

Figures 4, 5, 6, 7 and 8 show examples of the incremental computation of the cores by OIFT, from the ORFC cores, for a variety of real images. Next we define a measure to evaluate the robustness of the methods in relation to the seed positioning.
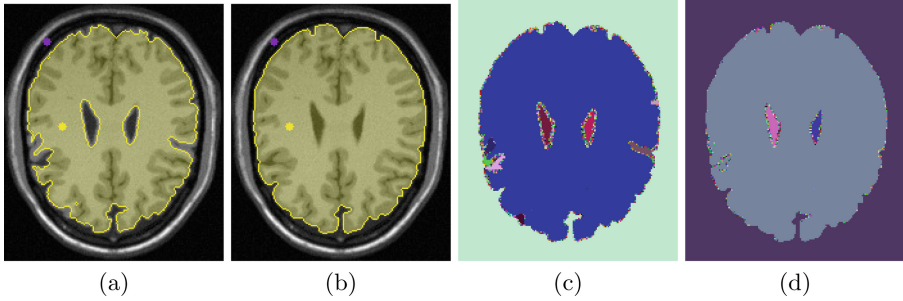

(a)   (b)   (c)   (d)

Fig. 4. A brain image from the BrainWeb - simulated brain database. (a) ORFC segmentation with RC = 99.95%. (b) OIFT segmentation with RC = 96.23%. (c) ORFC cores inside OIFT mask. (d) OIFT cores.

(a)   (b)   (c)   (d)

Fig. 5. Image of a license plate. (a) ORFC segmentation with RC = 97.89%. (b) OIFT segmentation with RC = 89.06%. (c) ORFC cores inside OIFT mask. (d) OIFT cores.
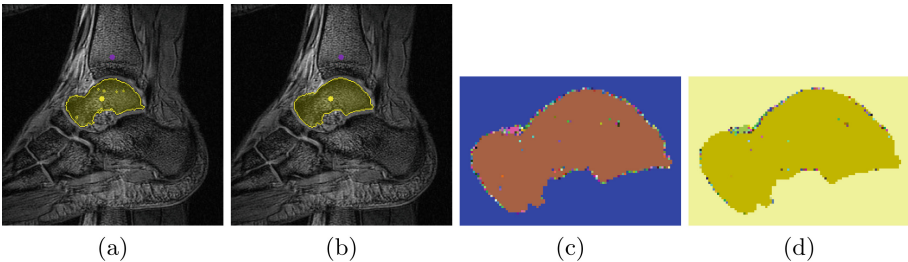

(a)   (b)   (c)   (d)

Fig. 6. MR image of a talus bone with good boundary contrast. (a) ORFC segmentation with RC = 98.60%. (b) OIFT segmentation with RC = 96.01%. (c) ORFC cores inside OIFT mask. (d) OIFT cores.
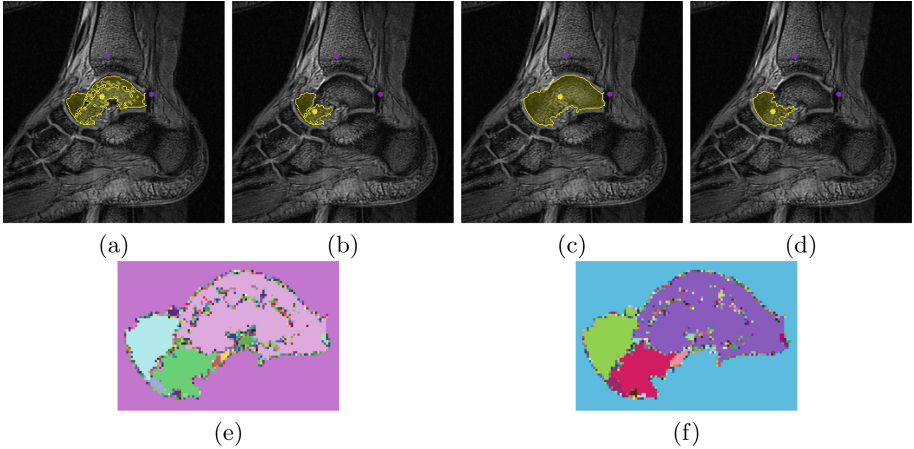
Fig. 7. MR image of a talus bone with poor boundary contrast. (a) ORFC segmentation with RC = 58.87%. (b) Effect of placing the seed outside its core. (c) OIFT segmentation with RC = 52.04%. (d) Effect of placing the seed outside its core. (e) ORFC cores inside the OIFT mask. (f) OIFT cores.
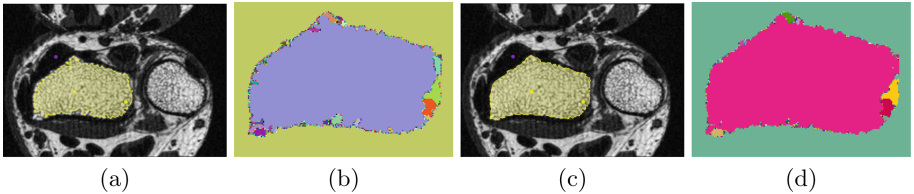

Fig. 8. An MR image of a wrist with two seed pixels selected inside the bone. (a) ORFC segmentation with RC = 99.17%. (b) OIFT segmentation with RC = 95.40%. (c) ORFC cores inside the OIFT mask. (d) OIFT cores.

For a given segmentation algorithm $A(\mathcal{S}_o, \mathcal{S}_b)$ with cores given by $\mathcal{N}(\mathcal{S}_o, \mathcal{S}_b)$, the *Robustness Coefficient* (RC) is defined as:

$$RC = \frac{|\mathcal{N}(\mathcal{S}_o, \mathcal{S}_b)|}{|A(\mathcal{S}_o, \mathcal{S}_b)|} \tag{5}$$

RC provides an analytic solution to measure the reproducibility of experiments. The higher the RC value, the lower is the sensitivity of the method in relation to inter- and intra-user variability in image segmentation. Note that a high RC value does not imply that the method has a high accuracy, the RC measure only evaluates how easy it is to reproduce the same segmentation, regardless of its accuracy. In this sense, it is a complementary measure to traditional accuracy measures.

In the experiments, we used 40 slice images from real MR images of the foot, to perform the segmentation of the bones talus and calcaneus, and 40 slice images from CT cervical spine studies of 10 subjects to segment the spinal-vertebra.

We used different seed sets automatically obtained by eroding and dilating the ground truth at different radius values. By varying the radius value, we can compute a segmentation for different seed sets and trace accuracy curves, using the Dice coefficient of similarity, and curves of the robustness coefficient. However, in order to generate a more challenging situation, we considered a larger radius of dilation for the external seeds (twice the value of the inner radius), resulting in an asymmetrical arrangement of seeds.

In order to show the robustness coefficient, we considered in the evaluation only methods with known procedure to compute their cores: $IRFC$ [10], RFC [26], $OIFT$ [17], $ORFC$ [3], or at least with a good lower bound estimation of their cores: $RFC + GC$ [11], $ORFC + GC$ [3], and $ORFC_{Core} + GC$ [28]. For $RFC + GC$ we considered $RC = \frac{|\mathcal{N}_{RFC}(\mathcal{S}_o, \mathcal{S}_b)|}{|A_{RFC+GC}(\mathcal{S}_o, \mathcal{S}_b)|}$, $RC = \frac{|\mathcal{N}_{ORFC}(\mathcal{S}_o, \mathcal{S}_b)|}{|A_{ORFC+GC}(\mathcal{S}_o, \mathcal{S}_b)|}$ for $ORFC + GC$, and $RC = \frac{|\mathcal{N}_{ORFC}(\mathcal{S}_o, \mathcal{S}_b)|}{|A_{ORFC_{Core}+GC}(\mathcal{S}_o, \mathcal{S}_b)|}$ for $ORFC_{Core} + GC$.

In the quantitative experiments, we adopted the weight assignment $\delta(a, b) = K - |G(a) + G(b)|$, where $G(a)$ denotes the gradient magnitude of the Sobel operator. For approaches based on directed graphs, we used $\alpha = -0.5$, for the foot bones (transitions from dark to bright pixels) and $\alpha = 0.5$ for the spinal-vertebra; and $\alpha = 0.0$ in the case of undirected approaches.
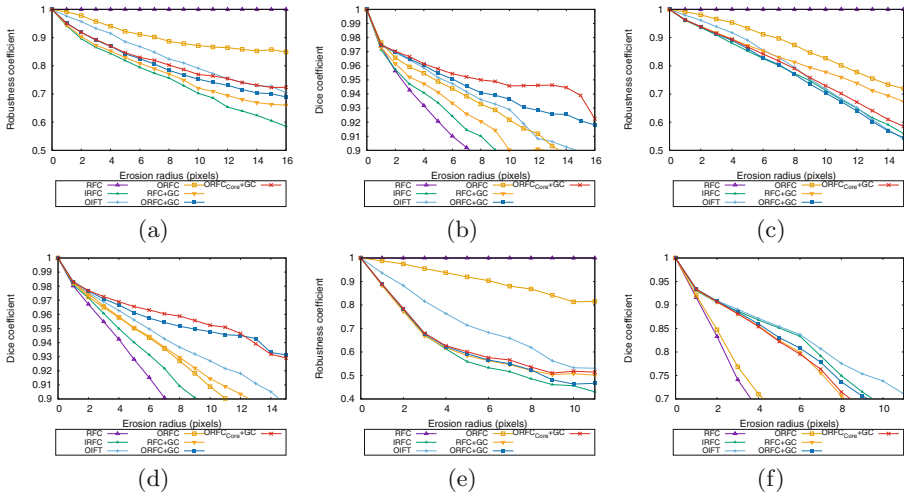

Fig. 9. The mean robustness coefficient curves and the mean accuracy curves (Dice coefficient), using non-equally eroded-dilated seeds, for segmenting: (a–b) talus, (c–d) calcaneus, and (e–f) spinal-vertebra.

Figure 9 shows the experimental results. Note that the robustness coefficient of RFC is always 100%, since $\mathcal{N}_{RFC}(\mathcal{S}_o, \mathcal{S}_b) = A_{RFC}(\mathcal{S}_o, \mathcal{S}_b)$ [26]. For the bones datasets, with respect to the Dice measure, $OIFT$ is among the first three methods, losing only to the hybrid methods $ORFC + GC$ and $ORFC_{Core} + GC$. However, with respect to the robustness coefficient, $OIFT$ usually gives better

results than $ORFC+GC$ and $ORFC_{Core}+GC$, losing only to RFC and $ORFC$. For the spinal-vertebra, the Dice values of all methods decrease rapidly because the object has thin parts and the erosion process rapidly eliminates seeds in several important regions of the object. $OIFT$ has the best Dice values for the spinal-vertebra, and the third best robustness coefficient. So we can conclude that $OIFT$ has a good balance between accuracy and robustness.

As future works, we intend to explore the cores of $OIFT$ to solve the inverse problem of image segmentation, in order to allow the user to interactively perform corrections on any segmentation mask.

References

1. Audigier, R., Lotufo, R.: Seed-relative segmentation robustness of watershed and fuzzy connectedness approaches. In: Proceedings of XX Brazilian Symposium on Computer Graphics and Image Processing (SIBGRAPI), pp. 61–68. IEEE CPS, Belo Horizonte, MG, October 2007
2. Bai, X., Sapiro, G.: Distance cut: interactive segmentation and matting of images and videos. In: Proceedings of IEEE International Conference on Image Processing, vol. 2, pp. II-249–II-252 (2007)
3. Bejar, H.H., Miranda, P.A.: Oriented relative fuzzy connectedness: theory, algorithms, and its applications in hybrid image segmentation methods. EURASIP J. Image Video Process. **2015**, 21 (2015)
4. Boykov, Y., Funka-Lea, G.: Graph cuts and efficient N-D image segmentation. Int. J. Comput. Vis. **70**(2), 109–131 (2006)
5. Boykov, Y., Kolmogorov, V.: An experimental comparison of min-cut/max-flow algorithms for energy minimization in vision. IEEE Trans. Pattern Anal. Mach. Intell. **26**(9), 1124–1137 (2004)
6. Couprie, C., Grady, L., Najman, L., Talbot, H.: Power watersheds: a unifying graph-based optimization framework. IEEE Trans. Pattern Anal. Mach. Intell. **99**(7), 1384–1399 (2010)
7. Ciesielski, K., Udupa, J.: Affinity functions in fuzzy connectedness based image segmentation i: equivalence of affinities. Comput. Vis. Image Underst. **114**(1), 146–154 (2010)
8. Ciesielski, K., Udupa, J., Falcão, A., Miranda, P.: Fuzzy connectedness image segmentation in graph cut formulation: a linear-time algorithm and a comparative analysis. J. Math. Imaging Vis. **44**(3), 375–398 (2012)
9. Ciesielski, K., Udupa, J., Falcão, A., Miranda, P.: A unifying graph-cut image segmentation framework: algorithms it encompasses and equivalences among them. In: Proceedings of SPIE on Medical Imaging: Image Processing, vol. 8314 (2012)
10. Ciesielski, K., Udupa, J., Saha, P., Zhuge, Y.: Iterative relative fuzzy connectedness for multiple objects with multiple seeds. Comput. Vis. Image Underst. **107**(3), 160–182 (2007)
11. Ciesielski, K.C., Miranda, P., Falcão, A., Udupa, J.K.: Joint graph cut and relative fuzzy connectedness image segmentation algorithm. Med. Image Anal. (MEDIA) **17**(8), 1046–1057 (2013)

12. Cousty, J., Bertrand, G., Najman, L., Couprie, M.: Watershed cuts: thinnings, shortest path forests, and topological watersheds. Trans. Pattern Anal. Mach. Intell. **32**, 925–939 (2010)
13. Falcão, A., Stolfi, J., Lotufo, R.: The image foresting transform: theory, algorithms, and applications. IEEE Trans. Pattern Anal. Mach. Intell. **26**(1), 19–29 (2004)
14. Grady, L.: Random walks for image segmentation. IEEE Trans. Pattern Anal. Mach. Intell. **28**(11), 1768–1783 (2006)
15. Lézoray, O., Grady, L.: Image Processing and Analysis with Graphs: Theory and Practice. CRC Press, California (2012)
16. Mansilla, L.A.C., Miranda, P.A.V., Cappabianco, F.A.M.: Oriented image foresting transform segmentation with connectivity constraints. In: IEEE International Conference on Image Processing (ICIP), pp. 2554–2558, September 2016
17. Mansilla, L., Miranda, P.: Image segmentation by oriented image foresting transform: handling ties and colored images. In: 18th International Conference on Digital Signal Processing, Greece, pp. 1–6, July 2013
18. Mansilla, L.A.C., Miranda, P.A.V.: Image segmentation by oriented image foresting transform with geodesic star convexity. In: Wilson, R., Hancock, E., Bors, A., Smith, W. (eds.) CAIP 2013. LNCS, vol. 8047, pp. 572–579. Springer, Heidelberg (2013). doi:10.1007/978-3-642-40261-6_69
19. Mansilla, L.A.C, Miranda, P.A.V: Oriented image foresting transform segmentation: connectivity constraints with adjustable width. In: XXIX Conference on Graphics, Patterns and Images, São José Dos Campos, SP, Brazil, pp. 289–296, October 2016
20. Miranda, P., Falcão, A.: Links between image segmentation based on optimum-path forest and minimum cut in graph. J. Math. Imaging Vis. **35**(2), 128–142 (2009)
21. Miranda, P., Falcão, A., Ruppert, G.: How to complete any segmentation process interactively via image foresting transform. In: 23rd SIBGRAPI: Conference on Graphics, Patterns and Images, pp. 309–316 (2010)
22. Miranda, P., Falcão, A., Ruppert, G., Cappabianco, F.: How to fix any 3D segmentation interactively via image foresting transform and its use in MRI brain segmentation. In: Proceedings of IEEE International Symposium on Biomedical Imaging (ISBI), Chicago, IL, pp. 2031–2035, April 2011
23. Miranda, P., Falcão, A., Udupa, J.: Synergistic arc-weight estimation for interactive image segmentation using graphs. Comput. Vis. Image Underst. **114**(1), 85–99 (2010)
24. Miranda, P., Mansilla, L.: Oriented image foresting transform segmentation by seed competition. IEEE Trans. Image Process. **23**(1), 389–398 (2014)
25. de Moraes Braz, C., Miranda, P.: Image segmentation by image foresting transform with geodesic band constraints. In: 2014 IEEE International Conference on Image Processing (ICIP), pp. 4333–4337, October 2014
26. Saha, P., Udupa, J.: Relative fuzzy connectedness among multiple objects: theory, algorithms, and applications in image segmentation. Comput. Vis. Image Underst. **82**(1), 42–56 (2001)
27. Singaraju, D., Grady, L., Vidal, R.: Interactive image segmentation via minimization of quadratic energies on directed graphs. In: International Conference on Computer Vision and Pattern Recognition, pp. 1–8, June 2008
28. Tavares, A.C.M., Bejar, H.H.C., Miranda, P.A.V.: Seed robustness of oriented relative fuzzy connectedness: core computation and its applications. In: Proceedings of SPIE on Medical Imaging, vol. 10133, Orlando, Florida, US, pp. 1013316–1013316-10, February 2017